Applied Energy 183 (2016) 1705–1721

Contents lists available at ScienceDirect

Applied Energy

journal homepage: www.elsevier.com/locate/apenergy

Wet impregnation of a commercial low cost silica using DETA for a fast post-combustion CO_2 capture process

C.F. Martín [a], M.B. Sweatman [b], S. Brandani [b], X. Fan [b,*]

[a] University of Aberdeen, School of Engineering, Fraser Noble Building, King's College, Aberdeen AB24 3UE, Scotland, United Kingdom
[b] Institute for Materials and Processes, School of Engineering, University of Edinburgh, Mayfield Road, Edinburgh EH9 3JL, United Kingdom

HIGHLIGHTS

- CO_2 capture capacity of silica gel was enhanced by 65% after impregnation by DETA.
- 10% DETA loading gives the best capture capacity and stability.
- Fast kinetics and stable cyclic CO_2 adsorption/desorption performance.
- Short cycle time and low regeneration temperature (60 °C).

ARTICLE INFO

Article history:
Received 14 June 2016
Received in revised form 30 August 2016
Accepted 26 September 2016

Keywords:
CO_2 capture
Adsorption
Amine
DETA
Impregnation
Thermal stability

ABSTRACT

This work presents an economic and simple method to manufacture low cost, but effective adsorbents for CO_2 capture through impregnating DETA to a low cost, porous silica gel. The results have demonstrated that the low cost silica gel impregnated by low molecular-weight amine is stable and work very well at a temperature up to 130 °C. The developed adsorbent has a fast adsorption kinetics and can be regenerated at a low temperature. This will significantly reduce the energy used to desorb CO_2, therefore the energy penalty. The effect of amine loading on the textural properties, thermal stability, and CO_2 capture performance of the impregnated silica gel is also reported in this paper. 10% amine loading gives the best porosity, stability and the highest adsorption capacity.

1. Introduction

Post-combustion CO_2 capture is considered as a promising solution to control CO_2 emissions from large fixed industrial sources. Post-combustion CO_2 capture processes include physical absorption [1,2], chemical absorption [3–5] adsorption with solid sorbents [6–9], and gas separation by membranes [10,11]. The most developed technology for post-combustion carbon capture is chemical absorption with aqueous alkanolamines (e.g. MEA, DEA, MDEA, DIPA) [5,12]. However the process is not completely ready for application to power plants because of several drawbacks, such as high equipment corrosion, amine degradation by SO_2, NO_2 and O_2 present in flue gases, high capital costs, high energy requirements for regeneration of amine absorbents, and low absorption efficiency [13–15].

Adsorption is considered a promising technology for many reasons, including the potential for high capacity and selectivity, fast kinetics, good mechanical properties of sorbents and stability after repeated adsorption-desorption cycles, and low corrosion of equipment [16–18]. A wide range of solid sorbents have been investigated for post-combustion capture, including carbon-based sorbents, zeolites, hydrotalcites, and metal-organic frameworks (MOFs) [16,19–25]. However, each type of adsorbent has its limitations for example, carbon-based sorbents and hydrotalcites tend to have low capacities and selectivities, while zeolites, hydrotalcites and MOFs suffer from poor performance in humid flue gases. Moreover, MOFs are not particularly robust and are still expensive [16].

Another option, introduced by Xu et al., is to try and combine the best features, and limit the worst, of amine absorption and solid adsorbents by incorporation of nitrogen functional groups within a solid material to increase specific adsorption sites. In general there are two different methods: physical impregnation of amine into porous materials, and chemical grafting of amine onto a porous material's surface. Normally, physical impregnation is

* Corresponding author.
E-mail address: x.fan@ed.ac.uk (X. Fan).

http://dx.doi.org/10.1016/j.apenergy.2016.09.081
0306-2619/

simply carried out by wet-impregnation with an amine-solvent mixture; the solvent is then evaporated after impregnation has occurred. The most common materials used for wet-impregnation are ordered mesoporous silicas due to their large surface area and pore volume, such as MCM-41 [26], MCM-48 [27], SBA-15 [28–33], SBA-16 [34], and KIT-6 [35]. PEI (polyethyleneimine) is the most commonly used amine for wet-impregnation due to its low volatility and hence good stability.

DETA, DIPA, AMPD, TEA, PEHA, TEPA, MEA, AMP, DEA and EDA have also been used in wet-impregnation studies. Table 1 summarises the CO_2 capture capacity, the drop in capacity after 4 consecutive adsorption-desorption cycles, and the amount of CO_2 desorbed after 10 min of regeneration, for a wide range of expensive and low cost support materials impregnated with different amine types (further discussion can be found in Section 4.3). "It indicate that the use of amines mainly focus on PEI, MEA, DETA, TEA, TETA. Impregnating tests have been focused on testing high molecular weight amines such as PEI as they are considered more stable. There is nothing done with DETA supported onto low-cost non-structured silica gel because DETA is a lower molecular weight amines. However, DETA combines primary and secondary amine groups (see the chemical structure in Fig. 1), has a small molecule size, low molecular weight (103.17 g mol^{-1}) and low viscosity, and therefore can be easily loaded into porous materials. Previous work on CO_2 absorption using bulk liquid DETA has demonstrated that it exhibits fast mass transfer rates, good CO_2 capture capacity, and a good cyclic capacity compared to other amines often used in absorption capture processes (e.g. MEA: methylethylamine) [36]. In addition, the heat of absorption for CO_2 in DETA is lower than for MEA [37], so the energy required for its regeneration should be lower.

Moreover, Zhao et al. have recently investigated the CO_2 uptake of DETA-impregnated titania-based sorbents, and microporous titania composite sorbents. They found that the CO_2 adsorption capacity of these adsorbents was higher than the analogous DETA-impregnated SBA-15 adsorbents [38,39].

Much of this previous work has focused on reaching the highest quantity of amine loaded into the structured and ordered mesoporous silica-based materials mentioned above. However, these silica materials are not yet made in large quantities and so are relatively expensive. Therefore, information about their regenerability and the drop in capture capacity is uncompleted. The present work provides insights into the use of moderate quantities of amine (DETA) loaded into a low-cost silica gel (its price is around 100 times cheaper (£99.20/kg) than structured commercial silica supports, such as MCM-48 (£10,750/kg) or KIT-6 (£11,250/kg) [40]. Overall, we produce a low cost and effective CO_2 adsorbent. However, due to its low molecular weight, DETA might leach or be degraded during the cyclic capture process. Therefore, this work also addresses the mechanisms of CO_2 capture in this material and its stability under repeated adsorption/desorption cycles.

2. Experimental section

2.1. Materials and sorbent preparation

The support material for liquid amine impregnation employed in this work was a micro and mesoporous commercial silica gel purchased from Fischer Scientific (S/0780/53) with a particle size in the range of 0.2–0.5 mm. Diethylenetriamine (DETA, Sigma-Aldrich, 99%) and methanol (Sigma-Aldrich, 99.8%) were used for sorbent preparation. Ultrahigh purity gases (>99.99%) were used for all measurements.

For the wet impregnation procedure, the desired amount of DETA was dissolved in 7 g of methanol under stirring for about 15 min, after which 3.5 g of silica gel was added to the solution. The resultant slurry was stirred for about 30 min, and then dried at 40 °C overnight (17 h) at atmospheric pressure [26,41,42]. The prepared adsorbents were denoted as FS-DETA-*X*%, where *X* represents the loading of DETA as a weight percentage of the original silica gel sample. The weight ratio of amine to silica was set at 0, 10, 20, 30, 40, and 80%, respectively. The methanol/silica weight ratio was 2:1 in all the samples.

2.2. Sorbent characterisation

The samples obtained were characterized in terms of specific surface area, porosity, pore size distribution, thermal stability and CO_2 capture performance.

2.2.1. Textural characterisation of the adsorbents

The prepared samples were characterized in terms of texture by means of N_2 adsorption/desorption isotherms at −196 °C. The N_2 isotherms were measured in a Quantachrome Autosorb iQ2 apparatus.

Prior to any measurement the samples were out-gassed for approximately 12 h under vacuum. The original silica gel sample (FS) was out-gassed at 110 °C with a heating rate of 5 °C/min. The wet impregnated samples were out-gassed at 30 °C with a heating rate of 1 °C/min.

The BET surface area (S_{BET}), total pore volume (V_p) and pore size distribution were determined from the N_2 isotherms at −196 °C before and after loading the DETA. The surface areas were calculated using the Brunauer-Emmett-Teller (BET) equation, and the pore volume (V_p) was calculated from the adsorbed nitrogen after complete pore condensation at $P/P_0 = 0.9905$ by applying the so-called Gurvich rule [43]. The pore size distribution was calculated by using the DFT method (slit pore, NLDFT equilibrium model) and the DA method for comparison.

2.2.2. Thermal stability of wet impregnated silica gel

The thermal and physical properties of the silica gel support before and after its impregnation with 10% of DETA were characterized by thermal gravimetric analysis (Q500 TGA from TA Instruments). About 35 mg of sample was heated under an inert atmosphere of N_2 (60 mL/min) up to 600 °C with a heating rate of 10 °C/min.

2.2.3. CO_2 sorption measurements

The capacity and kinetics of CO_2 adsorption of the silica gel before and after impregnation with DETA were measured with the thermogravimetric analyser (TGA). Pure CO_2 was used for the adsorption step, whereas pure N_2 was used as a purging gas for CO_2 desorption. In a typical experiment, 30 mg of adsorbent was placed in the crucible and heated up to 100 °C in a N_2 stream (60 mL/min) for 60 min to remove the CO_2 adsorbed from the air as well as all moisture. Afterwards the temperature was decreased to 25 °C and maintained for 120 min before changing the gas to CO_2. The adsorbents were then exposed to CO_2 for 250 min (60 mL/min). A temperature-programmed CO_2 adsorption test was then conducted with a slow heating rate of 0.5 °C/min from 25 °C to 100 °C. The CO_2 capture capacity at 25 °C was calculated from the weight gained after exposure to CO_2, and was expressed in mg of CO_2 per g of sorbent. The variation of capture capacity with temperature was obtained from the temperature-programmed CO_2 adsorption step (25–100 °C).

The cyclic adsorption capacity was also evaluated at 60 °C by means of 4 consecutives adsorption/desorption cycles in the TGA. Prior to the first cycle, samples were heated up to 100 °C in a N_2 stream (60 mL/min) for 60 min (drying step). Afterwards the temperature was cooled down to the desired temperature (60 °C) and

Table 1
Support materials and amines used for the surface modification by wet impregnation.

Samples	Amine (wt.%)		CO_2 adsorption capacity (mmol/g sorbent)			Gas composition	Drop in capacity after 4 cycles (%)	CO_2 desorbed after10 min-regeneration (mmol/g)		Reference
			25 °C	30 °C	75 °C					
Si-MCM-41	–	0	0.62	–	0.19	100% CO_2	–	–	–	Xu [55a,b], Son [35]
Si-MCM-41	PEI	30	–	–	1.56	100% CO_2	–	0.08	100% CO_2 (75 °C)/100% N_2 (100 °C)	
Si-MCM-41		50	0.75		2.52	100% CO_2	0.00 [g]	1.09	100% CO_2 (75 °C)/100% N_2 (75 °C)	
MCM-41		75			3.02	100% CO_2	–	–	–	
Silica Gel (Merck)	PEI	50	–	–	1.77	100% CO_2	–	–	–	
Cariat G10 Silica	PEI	67			2.65 (60 °C)	100% CO_2	1.52	0.01	100% CO_2 (60 °C)/100% N_2 (60 °C) (80 min cycle time)	Ebner [41]
KIT-6	PEI	50	1.91	2.21 (50 °C)	3.07	100% CO_2	0.85 (3rd and 1st cycle)	1.69	100% CO_2 (75 °C)/100% N_2 (75 °C)	Son [35]
								0.23	100% CO_2 (50 °C)/100% N_2 (50 °C)	
		30	–	–	1.45	100% CO_2	–	–	–	
		10	–	–	0.34	100% CO_2	–	–	–	
Carbon black	PEI	50	–	–	3.07	100% CO_2	–	–	–	Wang [65]
SBA-15	PEI	50		1.62 (45 °C)		15% CO_2				Sanz [33]
	PEI	50	0.83	1.70 (45 °C)	3.15 2.04	100% CO_2	0.86	–	–	Ma [38], Wang [65], Sanz, [31], Sanz-Perez [32]
	PEI	30	–	1.48 (45 °C)	–	100% CO_2	–	–	–	
SBA-AP [B]	PEI		–	1.88 (45 °C)	–	100% CO_2	–	–	–	
MC400/10[A]	PEI	83	–	–	4.45	10% CO_2	0.59[c] 0.47[d]	–	–	Qi [51]
Activated Alumina	PEI	40	0.93		1.50	100% CO_2	––	–	–	Plaza [66]
Activated Carbon	PEI	30	1.14	1.09	0.25	100% CO_2	18.37[h]	–	–	Plaza [62]
AC (BAC) [C]	–	0	–	1.55	0.62	100% CO_2	–	–	–	
AC (BAC)	PEI	15	–	1.10	0.58	100% CO_2	–	–	–	
AC (BAC)	PEI	25	–	0.75	0.53	100% CO_2	–	–	–	
AC (BAC)	PEI	50	–	0.70	0.35	100% CO_2	–	–	–	
TiNT	PEI	127	–	2.56	–	15% CO_2/N_2	–	–	–	
SBA-15	–	0		0.32	0.21	10% CO_2/N_2	–	–	–	Zhao [50]
SBA-15	DETA	10		1.22	0.85		–	–	–	
SBA-15	DETA	30		1.03	1.40		–	–	–	
SBA-15	DETA	50		1.41	2.75		–	–	–	
TiO_2 (C8-Ti)	DETA	10		1.17	0.78		–	–	–	
TiO_2 (C8-Ti)	DETA	30			2.30		30.87[D] 1.24[E e]	–	–	
TiO_2 (C8-Ti)	DETA	50			2.64		–	–	–	
Activated alumina	DETA	40	0.95		1.63	100% CO_2	–	–	–	Plaza [63]
FS (Silica Gel)	–	0	0.56	0.48	0.09	100% CO_2	–	–	–	This study
FS (Silica Gel)	DETA	10	0.91	0.88	0.44		0.36	0.57	100% CO_2 (60 °C)/100% N_2 (60 °C)	
FS (Silica Gel)	DETA	40	0.69	0.68	0.44		4.87	0.45		
Activated carbon	DETA	27	1.01	0.97	0.55	100% CO_2	12.5[h] (VSA)	–	–	Plaza [60]
AC	–	0	1.88	–	0.70	100% CO_2	–	–	–	
AC	MEA	51	1.02	1.55	1.70	100% CO_2	–	–	–	
AC	TEA	98% conc. in vol	0.32	–	0.27	100% CO_2	–	–	–	
AC	AMP	40	–	0.77	–	15% CO_2	–	–	–	
AC	MEA	40	–	1.11	–	15% CO_2	–	–	–	
TiO_2 (C8-Ti)	TETA	10	–	–	0.59	10% CO_2/N_2	–	–	–	Ma [38]
TiO_2 (C8-Ti)	TETA	30	–	–	1.80		–	–	–	
TiO_2 (C8-Ti)	TETA	50	–	–	2.24		–	–	–	
TiO_2 (C8-Ti)	TEPA	10	–	–	0.44		–	–	–	
TiO_2 (C8-Ti)	TEPA	30	–	–	1.53		–	–	–	
TiO_2 (C8-Ti)	TEPA	50	–	–	1.75		14.3[b]	–	–	
MT (MesoporousTiO_2)	Raw	0	–	–	0.84 (at 60 °C)	15% CO_2/N_2	–	–	–	
MT (MesoporousTiO_2)	TEPA	11	–	–	1.67 (at 60 °C)		–	–	–	

(*continued on next page*)

Table 1 (*continued*)

Samples	Amine (wt.%)		CO_2 adsorption capacity (mmol/g sorbent)			Gas composition	Drop in capacity after 4 cycles (%)	CO_2 desorbed after10 min-regeneration (mmol/g)		Reference
			25 °C	30 °C	75 °C					
MT (MesoporousTiO_2)	TEPA	24	–	–	1.92 (at 60 °C)		–	–	–	
MT (MesoporousTiO_2)	TEPA	31	–	–	2.52 (at 60 °C)		2.45 [f]	–	–	
MT (MesoporousTiO_2)	TEPA	40	–	–	2.17 (at 60 °C)		–	–	–	
SBA-15(P)[F]	*Raw*	0	–	–	0.05	100% CO_2	–	–	–	Yue [59]
SBA-15(P)	TEPA	50	–	2.10 (35 °C)	3.27	100% CO_2	8.42	–	–	
SBA-15	TEPA/DEA	35/15		–	4.00	100% CO_2	–	–	–	Yue [61], Choi [16]
SBA-15	TEPA	30	–	1.32 (45 °C)	–		–	–	–	Sanz-Perez [32]
SBA-AP[B]	TEPA	30	–	2.36 (45 °C)	–		–	–	–	
As-MCM-41	TEPA	60	–	–	5.39		–	–	–	Yue [60]
MC400/10[A]	TEPA	83	–	–	5.57	10% CO_2	1.60[c] 0.43[d]	–	–	Qi [51]
TiNT	TEPA	99.1	–	3.81	–	15% CO_2/N_2	1.25[a]	–	–	Song [24]
TiNT	Raw	0	–	0.92	–		–	–	–	
TiNT	EDA	90	–	1.09	–		–	–	–	
Zeolite 4A	–	0	3.07	–	–	100% CO_2	–	–	–	
Zeolite 13X	–	0	4.45	3.82	2.39	100% CO_2	–	0.05	100% CO_2 (75 °C)/100% N_2 (75 °C)	Son [35]
Zeolite 13X	MEA	0.2% (conc. in volume)	3.09	–	2.14	100% CO_2	–	–	–	
Zeolite 13X	MEA	50% (conc. in vol.)	1.45	–	1.41	100% CO_2	–	–	–	

[A] Mesoporous Silica Capsules.
[B] Double functionalisation: TEPA was impregnated over grafted SBA-AP.
[C] Bagasse-based activated carbon.
[D] Estimated after 4 cycles, considering the first cycle.
[E] Estimated after 4 cycles, without considering the first cycle.
[F] Water-washed SBA-15 without calcination.
[a] Adsorption: 100% CO_2 at 30 °C; Regeneration: 100% N_2 at 100 °C.
[b] Adsorption: 10% CO_2/N_2 at 75 °C; Desorption: 100% He, 1 h at 100 °C.
[c] Adsorption: 100% CO_2, 10 min at 75 °C; Regeneration: 100% N_2, 10 min at 100 °C.
[d] Adsorption: 100% CO_2, 25 min at 75 °C; Regeneration: 100% N_2, 25 min at 75 °C.
[e] Adsorption: 10% CO_2/N_2, 1 h at 75 °C; Regeneration: 100% He, 1 h at 100 °C.
[f] Adsorption: 15% CO_2/N_2 at 60 °C; Regeneration: 100% N_2 at 100 °C.
[g] Adsorption: 13% CO_2/4% O_2/13% H_2O/70%N_2, 240 min at 75 °C; Regeneration: 100% He, at 100 °C, 300 min at 75 °C.
[h] Drop measured after 3 vacuum swing adsorption (VSA) cycles. Adsorption: 100% CO_2, 25 °C, 30 min; Regeneration: vacuum, 30 min. Normal pressure recovery with an inert gas.

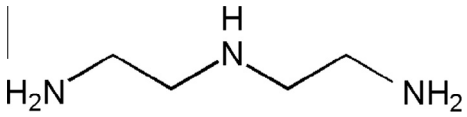

Fig. 1. Molecular structure of diethylenetriamine (DETA).

kept within the N_2 stream for 120 min before the change to CO_2 (60 mL/min) for another 120 min. The regeneration step was run by simple flushing of N_2 and the temperature was maintained constant at 60 °C. The total-cycle time was set at 240 min. The CO_2 capture capacity for each cycle was calculated from the mass gained by the samples after they were exposed to the pure CO_2 stream for 120 min. The initial mass was considered as the mass after the drying step for all the cycles.

3. Kinetic models description and solution methodology

Adsorption kinetic data of the prepared adsorbents is essential to understand the overall mass transfer of CO_2, as it will directly influence the duration of the adsorption process, the adsorber size requirements, consequently, the capital costs of the carbon capture unit. There is a wide variety of kinetic models with different degree of complexity in literature [44,45]. The most common approach to use these models is to fit the experimental data to the conventional kinetic models, and then select the model with the best fit. In this study, two of the most common theoretical kinetic models (pseudo-first-order and pseudo-second-order kinetic models) were employed to interpret the interactions between adsorbate and adsorbents, as well as the adsorption rate performance. Intraparticle diffusion model (IPD) was also employed to explore the CO_2 diffusion along the treated and non-treated amorphous silica support. The fitting of the models was done by using the adsorption data which is the initial stage (the first 70 s) of the curves in Fig. 2. After the 70 s, the temperature increase and the desorption procedure started.

3.1. Pseudo-first and pseudo-second order kinetic models

The pseudo-first-order kinetic model presumes reversible interactions between the gas and solid surface at equilibrium. The mechanism of adsorption involves chemical reaction between the CO_2 and the amine groups present on the adsorbent surface, and the rate of the change of the gaseous species is directly proportional to the difference between the adsorption capacity at

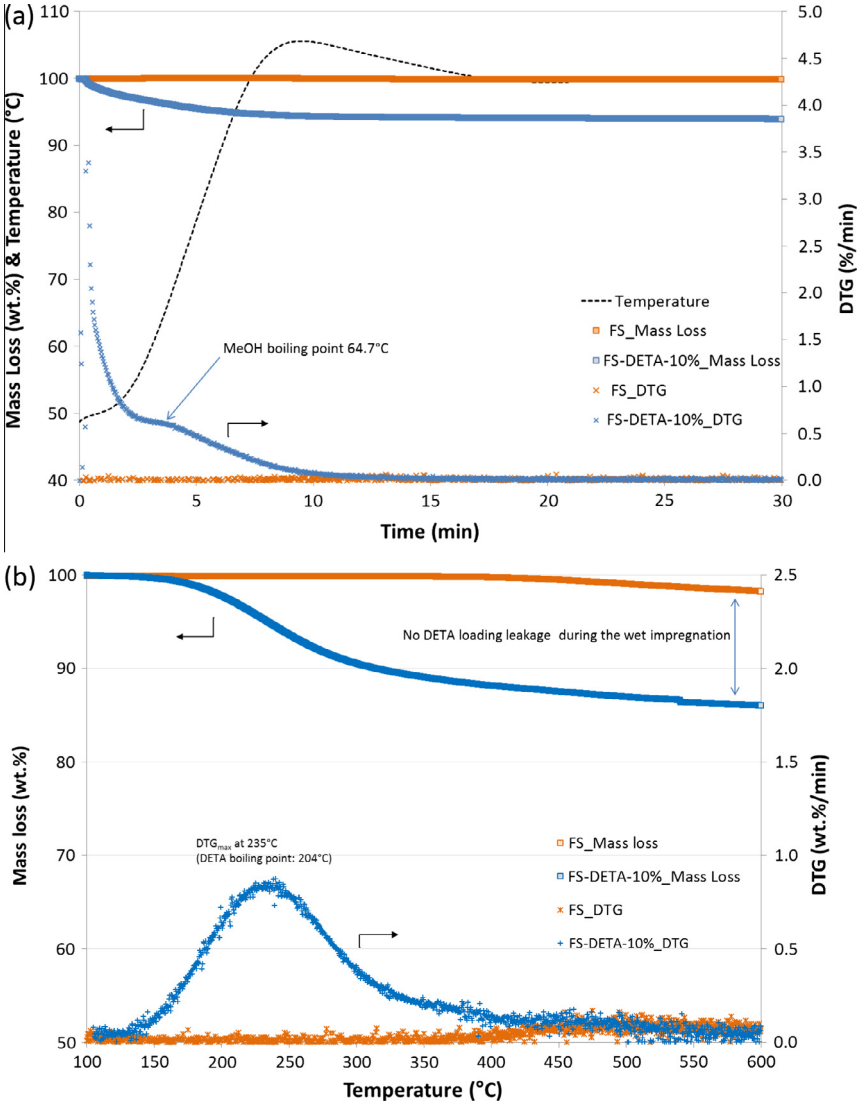

Fig. 2. Thermogravimetric profile versus time (a), and temperature (b) for pure silica gel (FS) and the amine loaded silica gel FS-DETA-10%.

equilibrium and the adsorption capacity at time t. The model is expressed as the following equation:

$$\frac{dq_t}{dt} = k_1(q_e - q_t) \quad (1)$$

where k_1 is the rate constant of pseudo-first-order adsorption (s^{-1}), q_e and q_t are the amount of CO_2 adsorbed (mol g^{-1}) at equilibrium and at time t (s), respectively. Integration of Eq. (1) considering the boundary conditions: $q_t = 0$ at $t = 0$ and $q_t = q_e$ at $t = t_\infty$, gives Eq. (2):

$$q_t = q_e(1 - e^{-k_1 t}) \quad (2)$$

The pseudo-second-order kinetic model (Eq. (3)) assumes that the overall adsorption kinetics is controlled by the chemical interactions, and that is the reason for the linear relationship that model describes between the adsorption rate and the square of the number of non-occupied adsorption sites.

$$\frac{dq_t}{dt} = k_2(q_e - q_t)^2 \quad (3)$$

where k_2 is the pseudo-second-order kinetic rate constant (mol g^{-1} s^{-1}). Integrating Eq. (3) for the same boundary conditions we obtain:

$$q_t = 1/(1/k_2 q_e^2) + t/q_e \quad (4)$$

Parameters k_1 and k_2 were obtained by minimising the sum of the squared errors between experimental and predicted values of q_t by using Solver. The goodness of fit of both kinetic models with the experimental data was evaluated by the root mean squared error (*RMSE*). The latter represents the error of the predicted values with the models and is calculated by the following expression:

$$RMSE\ (\%) = 100 \times \sqrt{\frac{\sum_{i=1}^{n}(q_{i,\mathrm{mod}} - q_{i,\mathrm{exp}})^2}{n}} \quad (5)$$

where n is the number of experimental adsorption points, q_{exp} and q_{mod} are the experimental and predicted values of amount adsorbed, respectively.

For the calculation of the rate constants, k_1 and k_2, the experimental q_e value was considered when fitting the models to the experimental kinetic data with the objective of getting the most realistic rate constant values.

3.2. Intraparticle diffusion model (IPD)

To complete the kinetic study of the adsorbent support prior and after the amine impregnation, CO_2 intraparticle diffusion during adsorption has been evaluated by employing the intraparticle diffusion model (IPD), proposed by Weber and Morris [46,47].

To apply the model, q_t (the amount of CO_2 adsorbed at any time) was plotted against $t^{1/2}$ (the square root of time) to get the straight line [48]. In this case, the multi-linearity in q_t vs. $t^{1/2}$ was observed. During the first step the instantaneous adsorption occurs on the external surface; the second step is when the gradual adsorption takes place, where intraparticle diffusion is controlled; and the third step is the final equilibrium step, where the adsorbate moves slowly from larger pores to micropores causing a slow adsorption rate.

The fractional approach to equilibrium change is done according to a function of $(D_t/r^2)^{1/2}$, where r is the radius of adsorbent particle and D is the effective diffusivity of adsorbate within the particle. The initial rate of IPD is obtained by linearization of the curve q_t $f(t^{1/2})$, which is expressed as:

$$q_t = k_d t^{1/2} + C \quad (6)$$

where k_d is the IPD rate constant (mol g^{-1} $s^{-1/2}$); C is a constant for any experiment (mol g^{-1}) which is normally positive, and indicats rapid adsorption occurring within a short period of time. The intercept C can be used to calculate the initial adsorption factor (R_i), defined by Feng-Chin et al. [49]. To calculate the initial adsorption behaviour, the following equation was used and subtracted from Eq. (6):

$$q_{ref} = k_d t_{ref}^{1/2} + C \quad (7)$$

where t_{ref} and q_{ref} are the longest time in the adsorption process and the solid phase concentration at time $t = t_{ref}$ for the adsorption system, respectively. Subtracting Eq. (7) by Eq. (6):

$$\frac{q_t}{q_{ref}} = 1 - R_i\left[1 - \left(\frac{t}{t_{ref}}\right)^{1/2}\right] \quad (8)$$

$R_i = (k_d\ t_{ref}^{\ 1/2}/q_{ref})$, which is defined as the initial adsorption factor of the IPD model. The well-known characteristic curve based on IPD model can be obtained from Eq. (8), and R_i can be calculated as:

$$R_i = 1 - \left(\frac{C}{q_{ref}}\right) \quad (9)$$

Accordingly, R_i can be expressed as the ratio of the initial CO_2 adsorbed amount (C) to the final adsorbed amount (q_{ref}).

The implication of the obtained initial adsorption behaviour will be analysed and described along with the characteristics curves based on the IPD model in Section 4.3.1.

In this work the second step of adsorption has been evaluated by the IPD model to further study the control of intraparticle diffusion on the CO_2 adsorption in relation with the amine loaded on the silica support. The goodness of fit of the IPD model with the experimental results was evaluated using the nonlinear coefficient of determination (R^2).

4. Results and discussion

4.1. Thermal stability of wet impregnated silica gel

Thermal stability and DETA loading were studied from the weight loss of the sorbents measured during the temperature-programmed desorption (TPD) experiments within the TGA. The evolution of the mass loss and the first derivative of the mass loss (DTG curve or mass loss rate) versus time (at 100 °C) and temperature (from 100 °C to 600 °C) are displayed in Fig. 2a and b respectively, for both the original silica gel (FS) and the impregnated FS-DETA-10%. For the pure silica gel support, the weight decrease started at 425 °C, and the total mass loss (2.1% at 600 °C) was gradual. In the case of FS-DETA-10%, the TG and DTG curves clearly show the existence of four thermal degradation regions: (i) 48–53 °C, (ii) 60–100 °C, (iii) 130–425 °C, and (iv) 425–600 °C. The first region was detected in the first 2 min of the experiment (see Fig. 2a). The second region was detected between the third minute and the 10th minute, with the maximum DTG observed at 67 °C after 4 min from the beginning of the experiment. The mass losses at a temperature up to 100 °C, which corresponds to the regions (i) and (ii), is attributed to the desorption of moisture and CO_2 previously adsorbed from the ambient, and to the evaporation of the solvent trapped in the pores during the wet impregnation procedure (methanol boiling point 64.7 °C). The third region of mass loss was detected with a sharp peak in the rate of weight loss in the temperature range from 130 °C to 425 °C (see Fig. 2b), and a maximum velocity of mass loss of 0.84 % min^{-1} was detected at 235 °C. The mass loss in the region (iii) is attributed to the evaporation of the amine (DETA boiling point 204 °C). After this maximum, further increase in temperature resulted in the loss of the remaining amine.

Finally, the last region of mass loss (iv) was observed from 425 °C to 600 °C and is attributed to degradation of the silica gel.

The total mass loss observed at 600 °C for FS-DETA-10% was 10.7%, discounting already the weight loss due to moisture and methanol in the previous regions at temperature below 130 °C (6.3%) and the total mass loss due to the degradation of the pure silica FS at 600 °C (2.1%). Therefore, this mass lost is almost equal to the amount of amine loaded into the silica gel. This confirms that the wet impregnation procedure is sound. The thermal stability exhibited by the FS-DETA-10% is in agreement with the results found by Zhao et al. for DETA-impregnated TiO_2 particles [50].

Zhao et al. reported that the molecular weight of the amine used affects the strength of interaction between the amine compounds and the support material, and hence amines with higher molecular weight evaporate at higher temperatures [39]. Considering the boiling point of the bulk DETA (204 °C), it can be observed from Fig. 2a and b that the thermal stability of the amine is increased when it is impregnated in the solid support material (maximum mass loss velocity at 235 °C). This occurs because DETA molecules strongly adhere to the porous surface of the silica gel, by either van der Waals forces or hydrogen bonding. Accordingly, it can be concluded that the studied DETA-impregnated silica gel displayed good thermal stability below 130 °C.

4.2. Textural properties from the N_2 isotherms

Nitrogen adsorption-desorption isotherms for silica gel before and after its impregnation with different DETA loadings are shown in Fig. 3. The corresponding surface area, total pore volume, micropore volume, and average pore diameter are summarised in Table 2. Figs. 4a and 4b show the pore size distribution (PSD) and the cumulative pore volume of FS, before and after the impregnation, calculated by the DFT method. Fig. 4c displays the PSD calculated by the DA method. Fig. 5 displays the BET surface area, total pore volume, and micropore volume as function of DETA loading (%).

The adsorption-desorption isotherms present a loop when $P/P_0 > 0.4$, and correspond to the type IV isotherm in the IUPAC classification. This type of isotherm is a typical characteristic of mesoporous solids, and the hysteresis loop is associated with capillary condensation in the larger mesopores. The total amount of N_2 adsorbed decreases with increasing amine loading into the silica gel support (Fig. 3). The PSD presented in Fig. 4a shows that the first peak of sample FS corresponding to micropores (diameter < 2 nm) is considerably reduced after impregnation with 10 wt.% of DETA. The PSD becomes narrower and centred at larger average pore size diameter ($D \sim 4.5$ nm) after impregnation because the amine preferentially fills micropores after impregnation. At higher amine loadings the micropores are completely filled and also the fraction of filled mesopores increases. Consequently, there is a significant reduction in pore volume and surface area (see Table 2 and Fig. 5) as amine loading increases, but the adsorption-desorption isotherm type is preserved as type IV for all the FS-DETA sorbents (Fig. 3). Thus, the available pore volume, V_p, and surface area were reduced from 0.52 cm^3/g to 604 $m^2\ g^{-1}$ respectively to a minimum of 0.06 $cm^3\ g^{-1}$ and 27 $m^2\ g^{-1}$ respectively after impregnation with 80% DETA, which indicates that

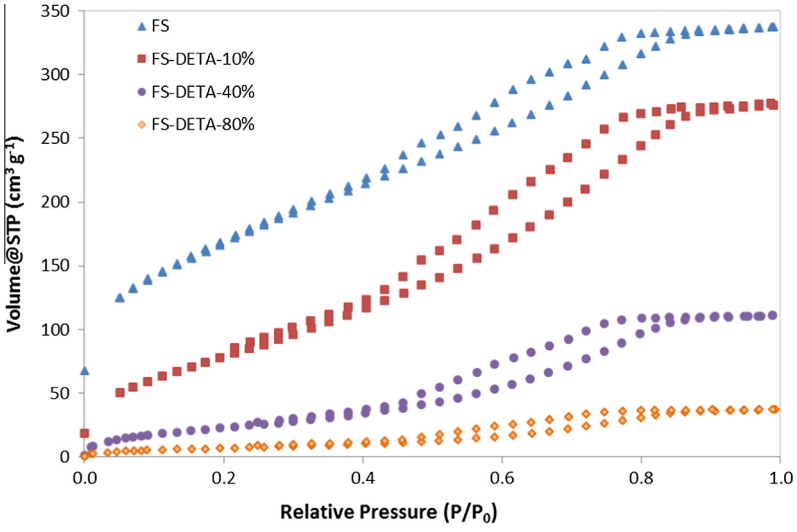

Fig. 3. N_2 adsorption/desorption isotherms at −196 °C for the silica materials before and after the wet impregnation with DETA.

Table 2
Textural parameters calculated from the N_2 isotherms at −196 °C.

Sample	S_{BET}[a]	P/P_0 range (S_{BET})	Correlation coefficient	V_p[b] (Gurvich)	DR[e]	DFT method[c]			DA[d]
	($m^2\ g^{-1}$)			(cm^3/g)	V_{micro} (cm^3/g)	V_p (cm^3/g)	V_{micro} (cm^3/g)	D (nm)	D (nm)
FS	603.8	5.22E−02-2.58E−01	0.99999	0.52	0.27	0.48	0.14	1.54	2.00
FS-DETA-10%	309.4	7.08E−02-2.58E−01	0.99969	0.43	0.13	0.40	0.01	4.54	2.36
FS-DETA-40%	90.2	7.02E−02-2.58E−01	0.99984	0.17	0.03	0.16	0.00	4.54	2.52
FS-DETA-80%	26.9	7.13E−02-2.58E−01	0.99965	0.06	0.01	0.05	0.00	4.15	2.56

[a] Surface area was calculated using the BET method at $P/Po = 0.05–0.26$.
[b] Total pore volumes (V_p) were evaluated using the Gurvitch's rule (GR) at $P/Po = 0.99$.
[c] Total pore volume (V_p), micropore volume (V_{micro}), mesopore volume (V_{meso}), and average diameter pore size (D) calculated by the DFT method.
[d] Average diameter pore size calculated by the DA Method. Micropores Analysis.
[e] Micropore volume (V_{micro}) calculated by Dubinin-Radushkevich Equation (DR) [66].

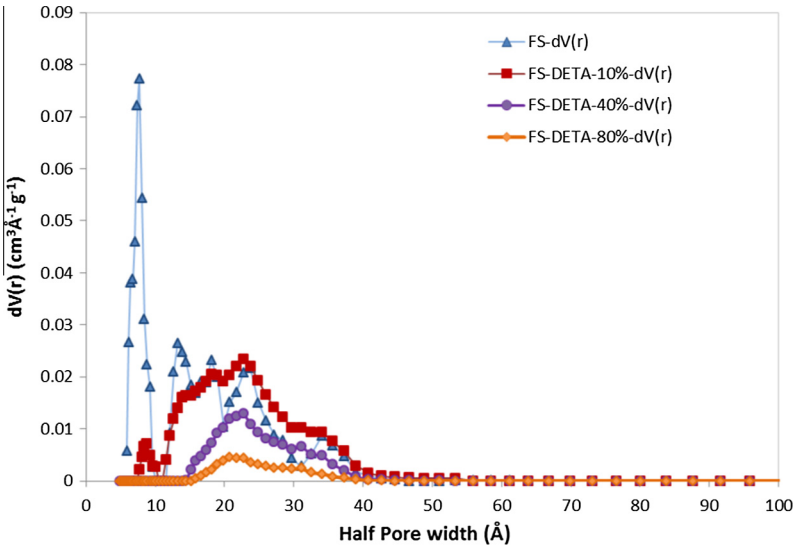

Fig. 4a. Pore size distribution (PSD) calculated from the N_2 isotherms at −196 °C by the DFT method.

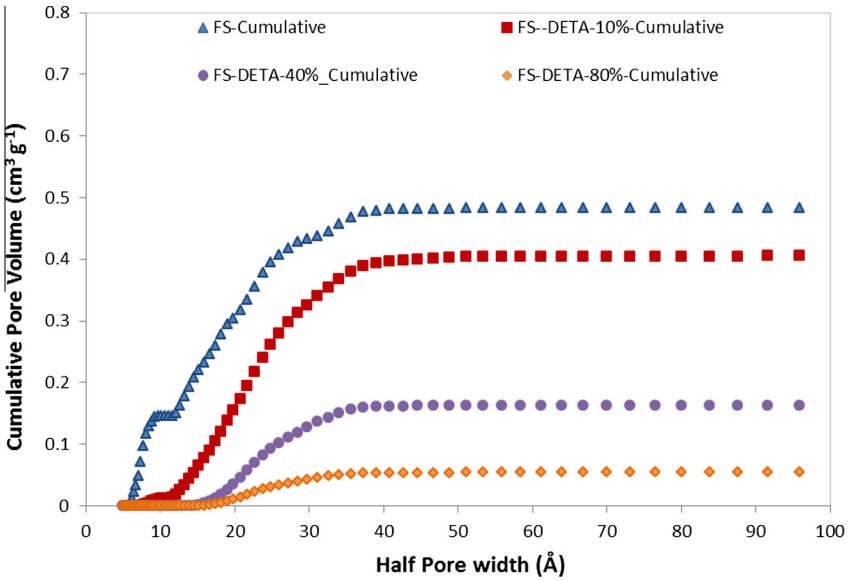

Fig. 4b. Cumulative pore volume calculated from the N_2 isotherms at −196 °C by the DFT method.

most of the original silica support pores were blocked with amine. Conversely, the considerable remaining porosity of FS-DETA-10% (V_p = 0.43 $cm^3\ g^{-1}$) could be beneficial for CO_2 diffusion and the adsorption-desorption process. The pore volume (V_p) decrease observed in Table 2 from the values estimated by the Gurvich's rule is in agreement to the cumulative pore volume ($cm^3\ g^{-1}$) estimated by the DFT method.

4.3. CO_2 adsorption-desorption study

In this section we evaluate the effect of DETA loading and temperature on the CO_2 capture capacity, the kinetics of CO_2 adsorption, and the cyclic performance of the FS-DETA series.

4.3.1. CO_2 capture capacity and kinetics

Fast adsorption and desorption kinetics are desired for CO_2 sorbents since a faster cycle time leads to smaller equipment and lower capital costs.

Fig. 6 shows the adsorption kinetics of CO_2 onto silica gel before and after its impregnation with different DETA loadings measured at 25 °C. It can be observed that CO_2 adsorption displays two different stages. Once the sorbents were exposed to the pure CO_2 stream (60 mL/min), a sharp weight gain occurred in less than 1 min, in which impregnated samples reached around 70% of their capacity. This fast process is then followed by a much slower adsorption process over the remaining 249 min in which the CO_2 uptake increased to the maximum observed (Fig. 7). This two-stage adsorption process showed similar trends in all the amine impregnated samples. For FS, CO_2 adsorption reached the maximum quickly, and the second stage was not obvious. The adsorption kinetics of samples prepared in this work, i.e. FS-DETA-10%, which reached 70% of its capacity after 47 s, is comparable with that reported for some other adsorbents in literature (i.e. KIT-6 impregnated with 50% PEI reached 70% of its capacity after 1 min [16]), but it is several times faster than many others, like the impregnated MCM-41-PEI-50%, which reached 70% of its capacity after

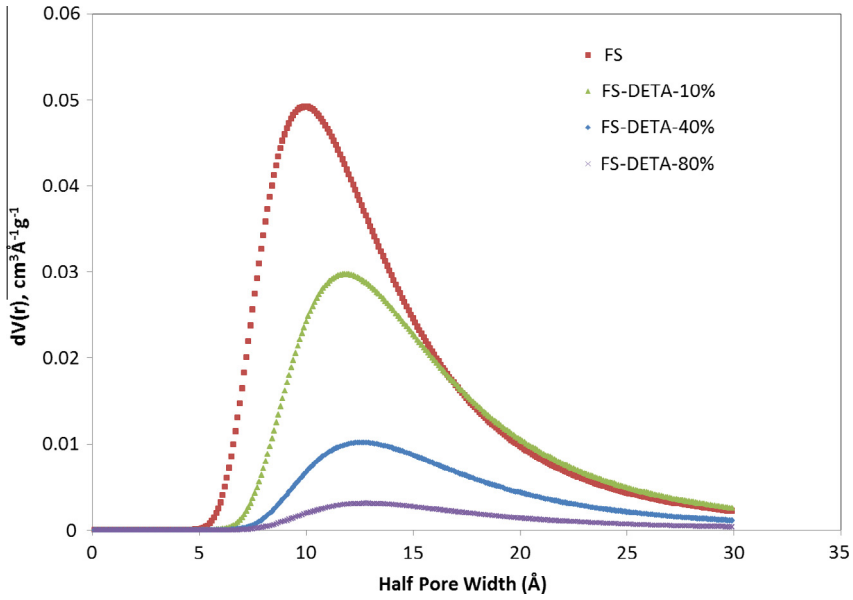

Fig. 4c. Pore size distribution (PSD) calculated from the N_2 isotherms at −196 °C by the DA method of micropore analysis.

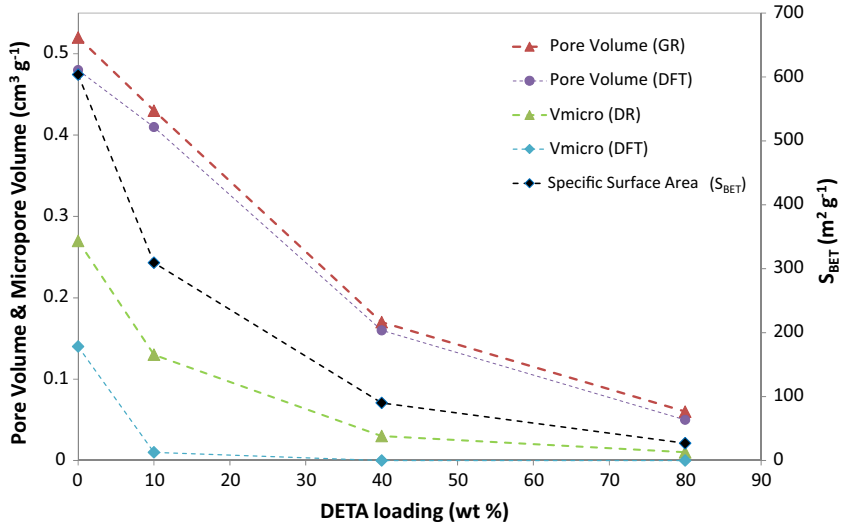

Fig. 5. The specific surface area (S_{BET}), pore volume and micropores volume of FS-DETA with different DETA loadings.

5.7 min [16,26,35,51], or the surfactant-promoted hierarchical porous silica (HPS) monoliths which completed the first stage in about 5 min [52]. Table 4 summarises the time taken to reach 50%, 70%, 80% and 90% of the maximum adsorption capacity for the most common PEI-loaded (50 wt.%) support materials, and the materials prepared in this work. Table 3 shows the time required for the regeneration of CO_2 in DETA-FS samples by flushing a N_2 stream at 60 °C. The 80% of the CO_2 was desorbed after 8–9 min flushing N_2 on FS-DETA-10%.

The rapid adsorption kinetics found in the first stage as well as the quick regeneration at relatively low temperature of the samples tested in this work, are considerable advantages for their practical applications in short adsorption-desorption cycles.

To study the kinetic of CO_2 adsorption, we have used three kinetic models to explain experimental results.

4.3.1.1. Pseudo-first and pseudo-second order kinetic models. Fig. 8 presents the experimental CO_2 uptake as function of time for the amine-impregnated and non-impregnated silica gel support at 25 °C, as determined using the gravimetric method, along with the corresponding profiles predicted by the pseudo-first and pseudo-second kinetic models. Table 5 summarises the values of the parameters of the kinetic models and the associated errors calculated by Eq. (5). Table 5 reveals that the kinetic rate for both models, k_1 and k_2, varied with the DETA loading. The favourable adsorption kinetics observed from the pseudo-first model for the 10% DETA loading (k_1 = 8.94E−02 s^{-1} for FS-DETA-10%) can be attributed to the faster diffusion of CO_2 molecules inside the pores, explained by the higher selectivity and chemical attraction towards the functionalised surface of the silica gel support. The increase in the mass transfer coefficient is not only reflected in the faster kinetics rate constant, k_1, but also in the sharper slope of the kinetic curves. However, for DETA loadings of 20% and 30%, the kinetic rate constant, k_1, decreased. The latter is attributed to the amine blockage of some pores fraction (in agreement with Fig. 5). Finally, for DETA loading 40% the highest kinetic rate

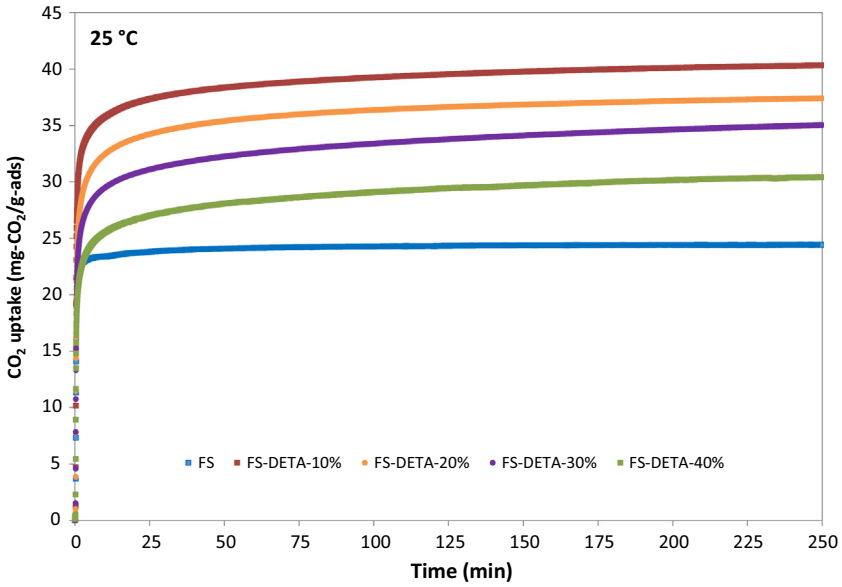

Fig. 6. Experimental CO_2 adsorption profiles of FS silica gel before and after the impregnation with DETA at different loadings. Conditions: 25 °C and 1 bar.

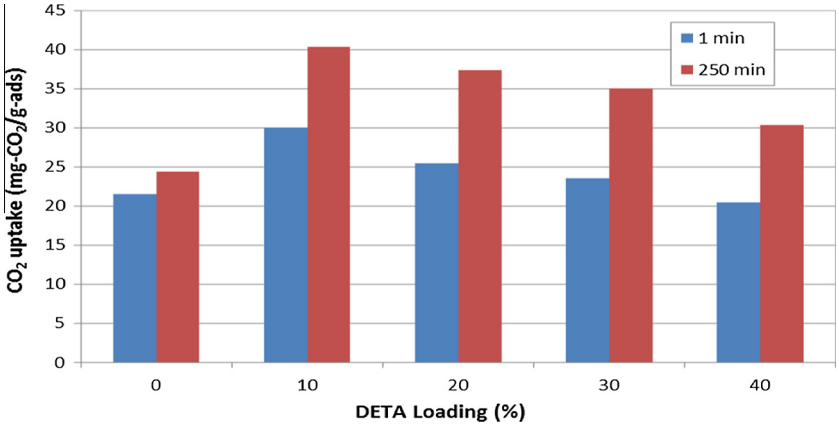

Fig. 7. CO_2 capture capacity of the low cost amorphous micro-mesoporous silica gel, before and after the impregnation with DETA at different loadings. Adsorption time effects on CO_2 capture capacity.

Table 3
Percentages of CO_2 desorbed at different times during the cycles and CO_2 working capacity for FS-DETA-10% and FS-DETA-40%, at 60 °C and 1 bar.

FS-DETA-10%				FS-DETA-40%		
Cycle	CO_2 desorbed %	Regeneration time min	Working capacity mg CO_2/g ads	CO_2 desorbed %	Regeneration time min	Working capacity mg CO_2/g ads
1	49.8	1.2	29.3	50.4	2.6	27.0
2	50.9	1.3	29.2	50.1	2.5	26.8
3	50.8	1.3	29.1	50.1	2.3	26.6
4	–	–		50.0	2.5	
1	80.0	8.4		80.0	26.9	
2	80.0	8.9		80.0	27.1	
3	80.0	9.0		80.0	24.6	
4	–	–		–	–	
1	90.0	31.7		90.0	82.2	
2	90.0	35.8		90.0	82.6	
3	90.0	36.5		90.0	72.1	
4	–	–		–	–	
1	96.2	120.0		93.3	120.0	
2	95.8	120.0		93.5	120.0	
3	95.6	120.0		94.6	120.0	
4	–	–		–	–	

Table 4
Time taken to reach certain percentage of the CO_2 capture capacity.

	Time taken to reach a specific percentage of the individual equilibrium CO_2 adsorption capacity (min)			
	50%	70%	80%	90%
MCM-41-PEI 50[a]	0.7	5.7	18.0	59.0
MCM-48-PEI 50[a]	0.7	1.7	11.0	53.0
SBA-15-PEI 50[a]	0.6	1.1	7.0	29.0
SBA-16-PEI 50[a]	0.5	1.7	7.1	28.0
KIT-6-PEI 50[1]	0.7	1.0	1.3	4.2
FS-DETA-10%[b]	0.4	0.8	2.0	13.5
FS-DETA-40%[b]	0.4	1.4	5.3	31.9

[a] Adsorption temperature: 75 °C Son [35].
[b] Adsorption temperature: 60 °C [This study].

constant value was k_1 = 9.06E−02 s^{-1}, which indicates that micropores were completely filled with DETA ($V_{micro} \approx 0.0$ cm^3 g^{-1} from Table 2).

It can be observed that pseudo-first-order kinetic model was fitted the entire adsorption period. In contrast, pseudo-second-order kinetic model overestimated the CO_2 uptake in the initial stage but underestimated it in the flatter region. As consequence, lower errors (RMSE, %) were observed for the pseudo-first-order kinetic model than for the pseudo-second-order kinetic model.

Results shown in Supplementary information (see Figure 1† and Table 1†) indicate that equilibrium adsorption capacities obtained experimentally ($q_{e,exp}$) and as predicted (q_e) by the pseudo-second-order kinetic model are overestimated, but in better agreement than the estimated by the pseudo-first-order kinetic model. The latter underestimated the equilibrium adsorption capacities. Furthermore better fittings were obtained for pseudo-second order kinetic model based on the higher R^2 values compared to the obtained for the pseudo-first-order kinetic model.

These results indicate that when experimental data was fitted with the models within the entire time range, and the equilibrium adsorption capacity value was estimated along with the rate constant value by using Solver, pseudo-second-order kinetic model gave better estimations. It is contrary to the best goodness of the pseudo-first-order kinetic model obtained for the first time interval (up to 80 s) fitted using experimental q_e values (see Fig 8 and Table 5).

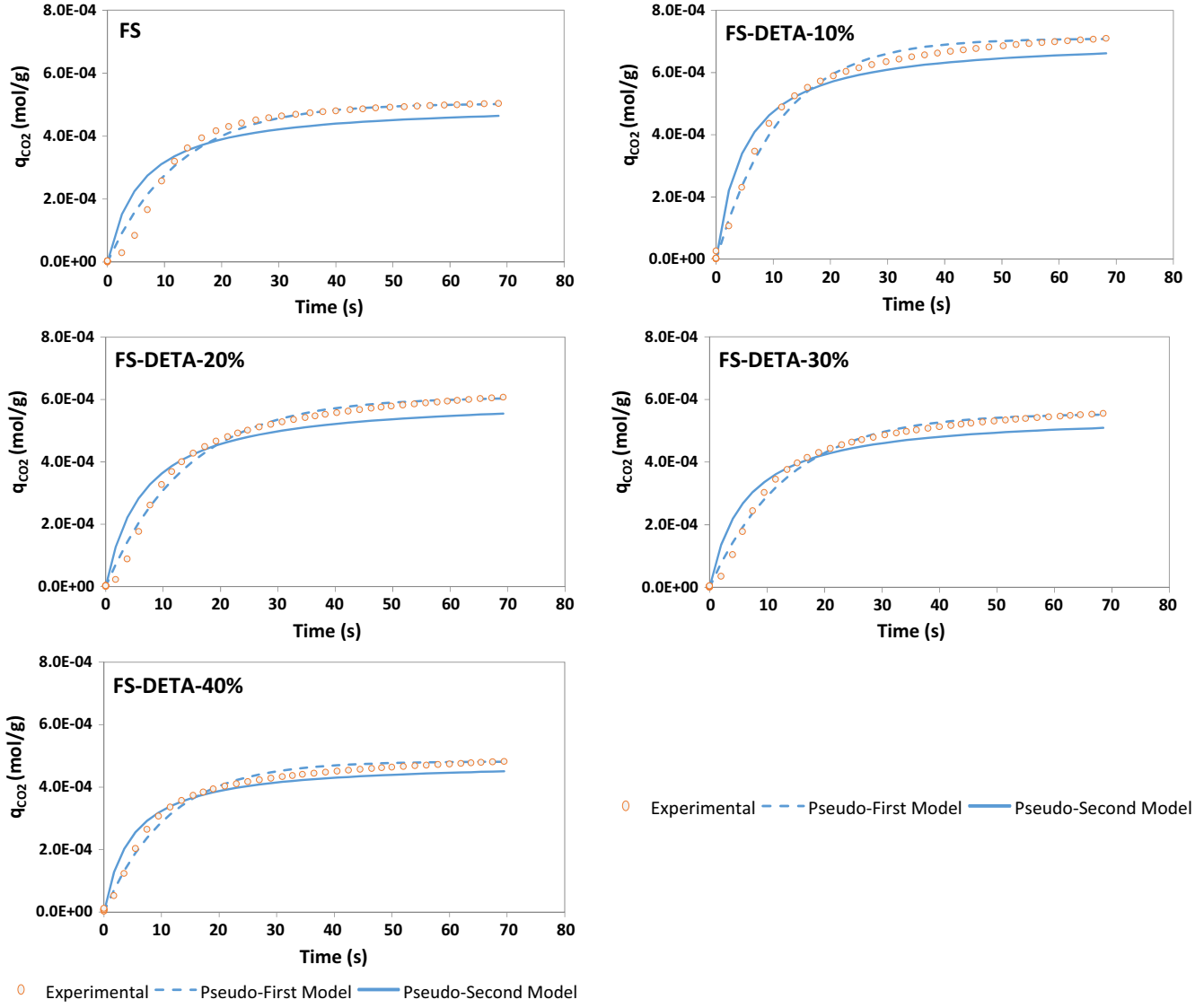

Fig. 8. Experimental CO_2 adsorption profiles of FS silica gel before and after the impregnation with DETA at different loadings, along with the corresponding fit to the pseudo-first and pseudo-second order kinetic models. Conditions: 25 °C and 1 bar.

Table 5
Calculated parameters of pseudo-first and pseudo-second kinetic models and associated RMSE (%) for CO_2 adsorption during the first 80 s of the adsorption experiment onto FS before and after the impregnation with DETA.

Sample		Pseudo-first order model		Pseudo-second order model	
	q_e (exp) (mol g^{-1})	k_1 (s^{-1})	RMSE (%)	k_2 (mol g^{-1} s^{-1})	RMSE (%)
FS	5.04E−04	7.93E−02	2.05E−03	3.39E+02	4.94E−03
FS-DETA-10%	7.09E−04	8.94E−02	1.77E−03	2.85E+02	3.97E−03
FS-DETA-20%	6.08E−04	7.12E−02	1.65E−03	2.50E+02	4.42E−03
FS-DETA-30%	5.55E−04	7.43E−02	1.39E−03	2.92E+02	3.95E−03
FS-DETA-40%	4.82E−04	9.06E−02	1.41E−03	4.24E+02	2.60E−03

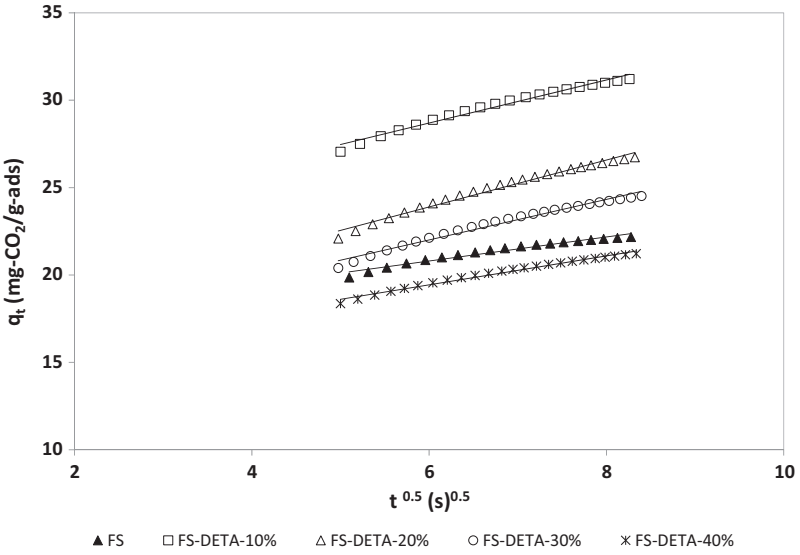

Fig. 9. Analysis of the adsorption kinetics of FS before and after its impregnation with DETA by IPD model.

Briefly, when experimental data is considered at the very first stage of the adsorption process (i.e. from 0 to 80 s) the model that best describes experimental data is the pseudo-first-order kinetic model. However, when the entire time-range for the experimental adsorption process is modelled, pseudo-second-order kinetic model better describes experimental results, indicating that adsorption process is controlled by the chemical interactions at longer exposition times of samples to CO_2.

4.3.1.2. Intraparticle diffusion model (IPD). The linearized plot of q_t vs. $t^{1/2}$ based on IPD model for the adsorption of CO_2 on the silica support before and after its impregnation is shown in Fig. 9, and the kinetic parameters of IPD model are summarised in Table 6. The model has been fitted to the second stage of the adsorption process that is characterized by a gradual adsorption in which intraparticle diffusion is controlled. None of the straight lines pass through the origin but present a positive intercept. It is because of the existence of instantaneous adsorption which implies that some amount of CO_2 molecules was adsorbed onto the exterior surface of the adsorbent in a short period of time. The intercept (C value) increases for the least impregnated sample, FS-DETA-10%, compared with the non-impregnated silica support, FS. However, it can be seen that initial adsorption decreases with increasing DETA-loading (%). The sample with the least impregnation loading (FS-DETA-10%) has the largest initial adsorption (C = 4.84E−04 mol g^{-1}), and the sample impregnated with the highest percentage of the amine, FS-DETA-40%, exhibits the lowest initial adsorption value (C = 3.29E−04 mol g^{-1}).

The slopes obtained for DETA-impregnated samples are higher than the slope obtained for the original support, FS. The slopes of FS-DETA-20% and FS-DETA-30% are close, revealing the very similar rates of IPD for the adsorption of CO_2 molecules. This observation is in agreement with the values obtained for the IPD rate constant, k_d (see Table 6).

To interpret the R_i values obtained based on IPD model (Table 6), the classification proposed by Feng-Chin et al. [49] has been

Table 6
Analysis of the adsorption of CO_2 on the silica support before and after its impregnation with DETA by IPD model.

Sample	Intraparticle diffusion model				
	K_d (mol g^{-1} $s^{1/2}$)	C (mol g^{-1})	R_i	Zone	R^2
FS	1.57E−05	3.79E−04	0.32	3	0.9629
FS-DETA-10%	2.80E−05	4.84E−04	0.47	3	0.9804
FS-DETA-20%	3.05E−05	3.60E−04	0.58	2	0.9826
FS-DETA-30%	2.63E−05	3.42E−04	0.57	2	0.9798
FS-DETA-40%	1.88E−05	3.29E−04	0.52	2	0.9857

Zone 3: Strongly initial adsorption; Zone 2: intermediately initial adsorption.

considered in this work. R_i is classified into four different zones depending on its value. When $1 > R_i > 0.9$ is called weakly initial adsorption (zone 1); $0.9 > R_i > 0.5$, intermediately initial adsorption (zone 2); $0.5 > R_i > 0.1$, strongly initial adsorption (zone 3); and $R_i < 0.1$, approaching completely initial adsorption (zone 4). The R_i values obtained for the samples prepared in this work correspond to zone 3 (strongly initial adsorption) for FS and FS-DETA-10%, and zone 2 (intermediately initial adsorption) for samples with higher amine loading, it is for FS DETA 20%, FS DETA 30% and FS DETA 40%, respectively. Lower impregnation percentage gives smaller R_i values, meaning that there is a stronger initial adsorption behaviour. In other words, when DETA loading increases the initial CO_2 adsorption does increase, it is due to the amine covering the walls of the pores but without blocking them (see V_p values from Table 2). Loadings from 20% up to 40% result in a lower initial adsorption capacity or higher R_i value (zone 2), which indicates some intraparticle diffusion limitation, that can be attributed to pore blocking by the amine. The adsorption in these systems occurs under intraparticle diffusion control in almost the whole process. Contrary for FS and FS-DETA-10% the kinetics of adsorption are controlled by the adsorption on the external surface speeded due to the higher attraction of the CO_2 molecule towards the amine groups, and also for the still-opened pore channels through which gas molecules travel. In practice, IPD model is suitable for the description of the present experimental data as the correlation coefficient ranges from 0.9629 to 0.9857.

4.3.2. Effect of DETA loading and temperature on the CO_2 capture capacity

4.3.2.1. DETA loading effect on CO_2 uptake. The CO_2 capture tests for the FS-DETA series (Fig. 6) showed that, in general, DETA impregnation can significantly increase the CO_2 adsorption capacity. The addition of 10 wt.% of DETA to the original silica resulted in an increase of 65% of CO_2 adsorption capacity at 25 °C (from 24.4 mg-CO_2/g-ads to 40.3 mg-CO_2/g-ads). However, the CO_2 adsorption capacity decreases with increasing DETA loadings after 10%. This is in agreement with the results reported previously for PEI-containing samples [51,53,54].

It is useful to compare with other support materials used for wet impregnation with amines. We see that the uptake of FS-DETA-10% (40.3 mg-CO_2/g-ads) is higher than the capacity of Si-MCM-41-PEI-50% (MCM-41 impregnated with PEI, 32.9 mg-CO_2/g-ads) reported previously by Xu et al. [55a] at the same conditions (100% CO_2, 25 °C and 1 bar). In that work the CO_2 adsorption capacity of the original silica MCM-41 (27.3 mg-CO_2/g-ads) was increased by 5.6 mg-CO_2/g-ads after the impregnation with 50 wt.% of PEI. In the present work, the quantity of amine added was much lower, 10 wt.%, and the CO_2 capture capacity increment with respect to the support material was nearly three times higher (16 mg-CO_2/g-ads). Accordingly, the amine efficiency in our prepared materials was much higher than that exhibited by the Si-MCM-41-PEI-50% under the same conditions.

Our results are also in line with those of Zhao et al. who impregnated SBA-15 with 10, 30 and 50 wt.% of DETA. They also obtained a lower CO_2 capture capacity for SBA-15-30% (45 mg-CO_2/g-ads) than for SBA-15-10% (53.68 mg-CO_2/g-ads) at 30 °C for a mixture of 10% (v/v) of CO_2 in N_2 at 1 atm [50]. This particular result is somewhat better than ours presented here given the lower partial pressure of CO_2 in their work, but the cost of the silica supports must also be taken into account.

4.3.2.2. Temperature effect on CO_2 uptake. The CO_2 adsorption performance of the impregnated materials at different temperatures gives essential information about the best temperature at which the sorbents should be used for CO_2 capture. As the reaction of amines with CO_2 is exothermic [56,57], an increase in temperature could reduce the capture capacity of the impregnated samples. Fig. 10 shows the CO_2 capture capacity with respect to temperature, in the range from 25 °C to 100 °C. We find the CO_2 capture capacity decreases with increasing temperature for all the studied samples, but there are small differences in the series. For instance, in the case of FS and FS-DETA-10%, the reduction of CO_2 uptake with temperature is faster than that obtained for FS-DETA-20% and FS-DETA-40%. The profile curves of FS-DETA-10% and FS-DETA 40% cross at 78 °C.

4.3.3. Cyclic adsorption-desorption performance

In order to avoid high energy penalty costs, apart from a high CO_2 capture capacity and a fast adsorption-desorption kinetics, CO_2 sorbents should be stable and regenerated at low temperature. In this section, the stability and cyclic behaviour of FS-DETA-10% and FS-DETA-40% were investigated via four consecutives CO_2 adsorption-desorption cycles, during 850 min at 60 °C. The

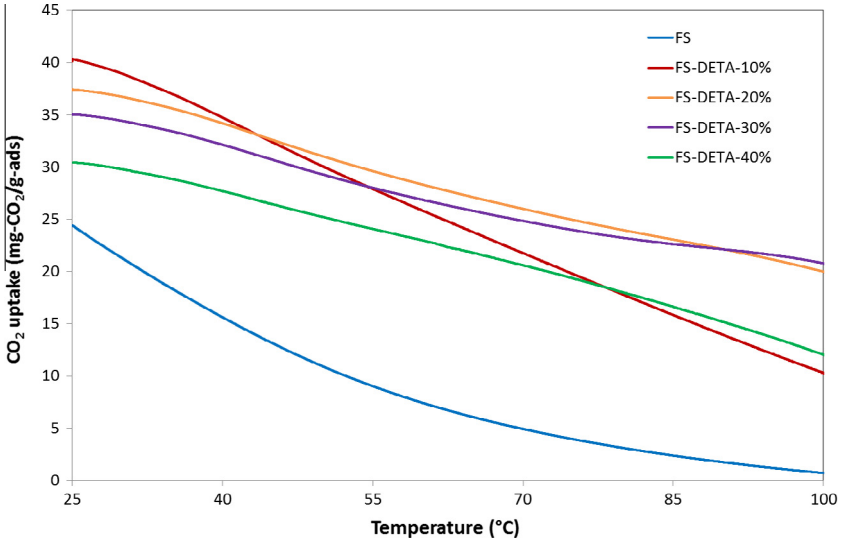

Fig. 10. Temperature-programmed adsorption of CO_2 of FS-DETA series. Conditions: 100% CO_2 at 60 mL/min flow rate, and 1 bar.

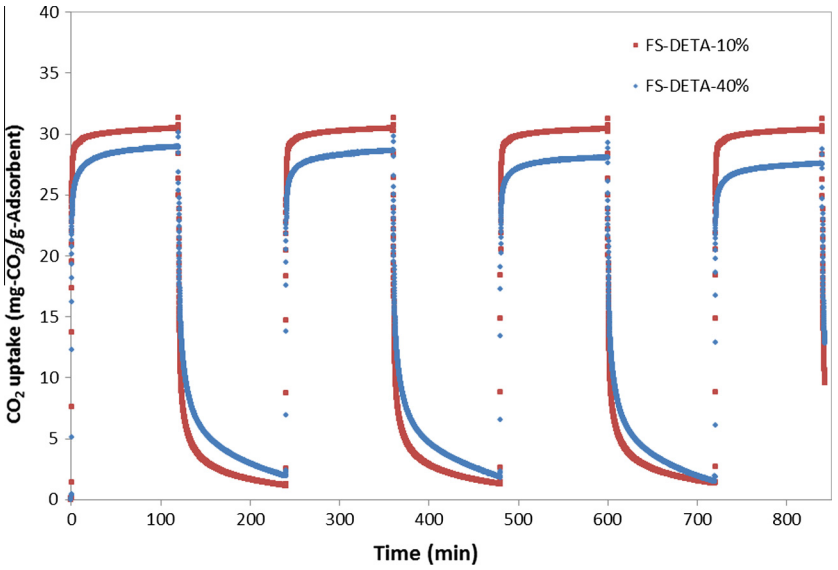

Fig. 11. CO_2 adsorption and regenerability of FS-DETA-10% and FS-DETA-40% at 60 °C. Adsorption step conditions: pure CO_2 (60 mL/min). Regeneration by flushing pure N_2 (60 mL/min).

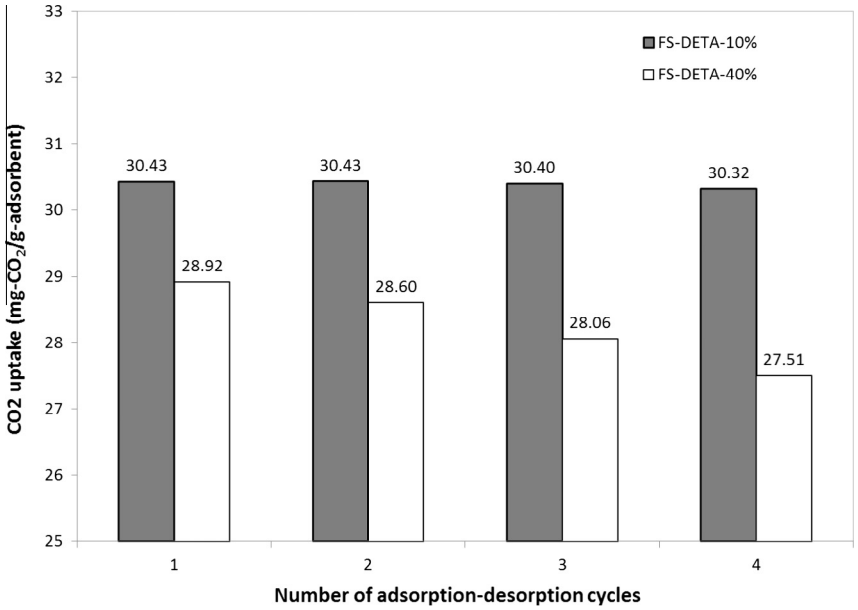

Fig. 12. CO_2 adsorption capacity of FS-DETA-10% and FS-DETA-40% respect to the number of cycles, at 60 °C and 1 bar.

adsorption temperature was selected at 60 °C since it is the most common temperature used in chemical absorption processes using aqueous alkanolamines. The carbon capture stability during the 4 cycles can be observed in Fig. 11, and the calculated CO_2 capture capacities during each cycle for FS-DETA-10% and FS-DETA-40% at 60 °C are shown in Fig. 12. The CO_2 capture capacity remained substantially constant after four cycles, with a relatively insignificant drop of 0.36% between the first and the fourth cycle in the case of FS-DETA-10% (from 30.43 to 30.32 mg-CO_2/g-ads). However, a drop of 4.9% in the CO_2 capture capacity between the first and the fourth cycle was observed for FS-DETA-40% (from 28.92 to 27.51 mg-CO_2/g-ads). The drop exhibited by FS-DETA-40% could be due to imperfect regeneration, or possibly leaching of DETA from the support material during the adsorption or regeneration processes. For comparison, a drop of 4% in the carbon capture capacity after 10 cycles was considered acceptable for MC-PEI-65% by Jitong and Wang [58], whereas a drop of 7% in the carbon capture capacity observed on 50-TEPA-TiO_2-Based composite sorbents under 10% CO_2/N_2 at 75 °C was associated with the continuous volatilisation of the impregnated TEPA during the first 4 cycles [38].

Regeneration of FS-DETA-10% also occurs more quickly than for FS-DETA-40%. From Fig. 11 and Table 3 we see that 50% of the adsorbed CO_2 was rapidly desorbed from FS-DETA-10% after purging for 1.2 min, and desorbed from FS-DETA-40% after purging for 2.5 min. Moreover, 80% of the CO_2 was released from FS-DETA-10% after 8 min of purging, and was released from FS-DETA-40% after 27 min of purging. Essentially, desorption rates peak during the first minute and a slow tail is displayed afterwards for both samples (see Fig. 11).

This observation agrees with the influence of temperature on the rate of CO_2 uptake observed in the CO_2 temperature-programmed adsorption experiments explained in Section 4.3.2.

Table 3 shows the working capacity calculated by the difference of CO_2 capture at the 120-minute adsorption and desorption steps. It is almost constant for each cycle for FS-DETA-10%, while a slight decrease with each cycle, in the region of 1.5% per cycle, is observed for FS-DETA-40%. Once again, this gradual decrease could be caused by incomplete regeneration of the sorbent after each cycle or by leaching of amine from the sorbent.

4.3.3.1. Materials' comparative discussion based on the CO_2 adsorption-desorption study. In Table 1 can be observed that modified as-prepared mesoporous silica SBA-15 (SBA(P)) with 50% TEPA loaded leads to a remarkably high adsorption capacity (3.27 mmol/g) for this mesoporous silica–amine composite. Even higher capacities are found for TEPA-impregnated As-MCM-41-TEPA-60% (5.39 mmol/g), mesoporous silica capsules MC400/10-TEPA-83% (5.57 mmol/g) at 75 °C and 1 bar CO_2 partial pressure, and TEPA/DEA-impregnated SBA-15 (5.57 mmol/g) at 75 °C and 0.1 bar CO_2 partial pressure [51,59–61]. However, MC400/10-TEPA-83% lead to a drop of 60% of the CO_2 capacity after 50 cycles [51], and TiO_2 (C8-Ti)-TEPA-50% lead to the highest drop observed in the table after 4 TSA cycles (14.4%) [38]. Consequently, stability of materials impregnated with TEPA is the biggest problem for these high-capacity materials.

In contrast, the lowest CO_2 capture capacity drop after 4 cycles was observed with Si-MCM-41-PEI-50% (almost zero percentage) and with FS-DETA-10% (0.36%) prepared in this work. Accordingly, DETA-impregnated amorphous silica gel prepared in this study shows very good stability and it can be compared with the support materials impregnated with the most stable amine (PEI).

The capture capacity exhibited by the materials prepared in this study is similar to that obtained by DETA-impregnated activated alumina (25 °C), TiO_2 (C8-Ti)-TEPA-10% (75 °C), and activated carbon AC-TEPA-10% (75 °C), but higher than that displayed by Si-MCM-41-PEI-50% at 25 °C, and the activated carbons: AC-TEA (all temperatures measured), AC-AMP (30 °C), AC(BAC)-PEI-50% (all temperatures measured), AC-PEI-30% (75 °C) and AC(BAC)-PEI-25% (30 °C) (see Table 1).

Although the capture capacity for the materials prepared in this study is not as high as for the structured silicas (i.e. MCM-41, SBA-15 or KIT-6), FS-DETA-10% and FS-DETA-40% present very easy and fast regeneration of CO_2 after 10 min flushing N_2 without an increase of the temperature. The amount of CO_2 desorbed after 10 min flushing N_2 at 60 °C for FS-DETA-10% (0.57 mmol/g) and FS-DETA-40% (0.45 mmol/g) is higher than that obtained for Si-MCM-41-PEI-30% by passing N_2 at 100 °C (0.08 mmol/g), Cariat G10 Silica-PEI-67% (0.01 mmol/g) at 60 °C, KIT-6-PEI-50% (0.23 mmol/g) at 50 °C and zeolite 13X (0.05 mmol/g) at 75 °C (see Table 1). Regeneration of impregnated silicas prepared in this work can be achieved in a matter of minutes: i.e. 2 min were required to desorb the 80% of the CO_2 from FS-DETA-10% at low temperature (60 °C) (see Table 4).

Among the variety of amines tested on commercial low cost supports, DETA-impregnated activated carbon and aluminium oxide showed the highest capture capacity of the series (1.01 mmol/g and 0.95 mmol/g at 25 °C, respectively) [62,63]. In the current study, FS-DETA-10% shows similar capacity (0.91 mmol/g) to DETA-impregnated alumina loaded with 40%, but slightly lower than activated carbon loaded with 27% DETA (1.01 mmol/g). However, the drop in capacity measured on the DETA-impregnated activated carbon (12.5%) resulting after 3 vacuum swing adsorption (VSA) cycles is high, and not comparable at all with the drop in capacity after TSA cycles presented in Table 1.

Briefly, the low cost silica used in this work present similar CO_2 capture capacity as some low cost supports such as commercial activated carbons, activated aluminas and silicas impregnated with low molecular weight amines. Moreover, the stability and regenerability displayed by the FS-DETA series seems to be reasonably favourable.

4.4. Interpretation of results

Here we present a consistent interpretation of all these results. We should first mention that the FS material used here is expected to consist of packed and fused silica nanospheres, in the region of 5 nm in diameter. This type of structure leads naturally to the appearance of micropores, formed by the 'wedges' between adjacent spheres, and mesopores that represent longer range packing structure. Also, it is known that the reaction of amines with CO_2 in the absence of water leads to the formation of carbamate and hydronium ion pairs. Due to their ionic nature, these reaction products are likely to be more viscous, and perhaps even solid, at high conversions relative to the reactants.

A widely accepted mechanism for wet impregnation of silica by amines is that amines diffuse into the pore space of the solid support and interact with hydroxyls on the silica surface, establishing hydrogen bonds. This presents as strong surface adsorption, leading to the preferential filling of micropores with amine at low loadings. Larger pores are gradually filled with increased amine loading. This is entirely consistent with the PSDs observed in Fig. 4a. Due to the strong amine-silica interaction, and the cooperative effect of adjacent pore walls in micropores, the amine in these micropores is relatively stable with very low vapour pressure and evaporation from the pore. Thus, leaching from micropores at low amine loadings is much reduced compared to the rate of leaching from mesopores at higher amine loadings.

However, it is also important to consider pore connectivity and pore accessibility. When only micropores are filled, i.e. when the wedges between silica nanospheres are filled, there is little effect on the pore connectivity or accessibility. However, as the proportion of filled mesopores increases, more and more of the pore network becomes blocked by amine and inaccessible to gases with poor diffusion through the amine. When CO_2 is introduced into the material, it reacts with surface layers of amine leading to the production of more viscous reaction products. The diffusivity of CO_2 can be assumed to be reduced in these layers, leading to a slowing down of kinetics. Therefore, as the loading of amine increases, less and less pore space is effectively available to CO_2 due to kinetic restrictions. In principle, the equilibrium adsorption of CO_2 should increase with increasing loading of amine. However, the reduced availability of pores and worsening kinetics prevent this.

Consequently, two kinetic processes with very different timescales are observed for CO_2 adsorption and desorption. CO_2 absorption occurs quickly into the outer surface of amine leading to the formation of viscous reaction products. The topology of this surface coarsens with increased amine loading, leading to reduced CO_2 uptakes at short times with increased amine loading. The second process is slow diffusion of CO_2 or carbamate through this surface to the less accessible regions of the pore network. The same processes operate in reverse during desorption. This kind of two-stage adsorption-desorption process has been reported before in other impregnated sorbents [51,52,55].

At higher temperatures two key effects combine to produce the observed results. First, higher temperatures lead to lower equilibrium CO_2 capture due to the exothermic nature of the reaction of amines with CO_2. However, there is improved diffusion of CO_2 through DETA-filled pores because of the lower DETA viscosity at higher temperature. Consequently, the CO_2 capacity appears to

decrease more slowly with increasing temperature for higher amine loadings.

5. Conclusions

The carbon capture characteristics of low cost diethylenetriamine (DETA) impregnated amorphous silica gel has been reported in this work for the first time. The composite material was found to be stable at temperatures below 130 °C. The CO_2 capture capacity was enhanced by 65% after impregnation of the amorphous silica support with 10 wt.% of DETA. Reduced performance in every respect was found at higher loadings. We interpret this reduced performance in terms of increased pore-blocking by DETA with increasing DETA loading.

Although low molecular weight amines have previously been reported as unsuitable for post-combustion CO_2 capture applications due to poor stability, this work has demonstrated that a low cost silica gel impregnated with 10 wt.% of DETA displays fast kinetics and relatively stable cyclic CO_2 adsorption/desorption performance, at least over 4 cycles. Additionally this work has demonstrated that regeneration of the FS-DETA-10% is easily and rapidly reached by only flushing with N_2, with no need to increase the temperature. Nevertheless a further study needs to be done in order to optimise the regeneration conditions for the best cyclic performance.

In conclusion, fast kinetics and the cyclic stability make DETA impregnated silica gel a promising candidate in cyclic CO_2 capture processes. The short cycle time and low regeneration temperature (60 °C), which is significantly lower than the temperature typically used to regenerate solid amine sorbents, normally in the range of 100–140 °C [64], imply potential energy savings. Additionally, the advantage of the wet impregnation procedure over the amine grafting is its simple route of preparation, i.e. the complex and expensive multi-step preparation of grafted amines is avoided here. Moreover, the estimated total cost of preparation of these materials could be much lower due to the low cost of the materials used.

All of these results are very promising and make these DETA impregnated silica gels as candidates for further study for their potential application in cyclic adsorption-desorption post-combustion CO_2 capture processes to serve power and industry.

Acknowledgements

We acknowledge EPSRC for the Grants EP/J019720/1 and EP/J019704/1.

Appendix A. Supplementary material

Supplementary data associated with this article can be found, in the online version, at http://dx.doi.org/10.1016/j.apenergy.2016.09.081.

References

[1] Chiesa P, Consonni SP. Shift reactors and physical absorption for low-CO_2 emission IGCCs. J Eng Gas Turbines Power 1999;121:295–305.
[2] Littel RJ, Versteeg GF, van Swaaij WPM. Physical absorption into non-aquaous solutions in a stirred cell reactor. Chem Eng Sci 1991:463308–13.
[3] Aroonwilas A, Veawab A. Characterization and comparison of the CO_2 absorption performance into single and blended alkanolamines in a packed column. Ind Eng Chem Res 2004;43:2228–37.
[4] Bishnoi S, Rochelle GT. Absorption of carbon dioxide into aqueous piperazine: reaction kinetics, mass transfer and solubility. Chem Eng Sci 2000;55:5531–43.
[5] Rochelle GT. Amine scrubbing for CO_2 capture. Science 2009;325:1652–4.
[6] Chang FY, Chao KJ, Cheng HH, Tan CS. Adsorption of CO_2 onto amine-grafted mesoporous silicas. Sep Purif Technol 2009;70:87–95.
[7] Harlick PJE, Tezel FH. An experimental adsorbent screening study for CO_2 capture from N_2. Microporous Mesoporous Mater 2004;76:71–9.
[8] Martín CF, García S, Pis JJ, Rubiera F, Pevida C. Doped-phenol-formaldehyde resins as precursors for precombustion CO_2 capture adsorbents. Energy Procedia 2011;4:1222–7.
[9] Martín CF, Plaza MG, García S, Pis JJ, Rubiera F, Pevida C. Microporous phenol-formaldehyde resin-based adsorbents for pre-combustion CO_2 capture. Fuel 2011;90:2064–72.
[10] Ebner AD, Ritter JA. State-of-the-art adsorption and membrane separation processes for carbon dioxide production from carbon dioxide emitting industries. Sep Sci Technol 2009;44(6):1273–421.
[11] Powell CE, Qiao GG. Polymeric CO_2/N_2 gas separation membranes for the capture carbon dioxide from power plant flue gases. J Membr Sci 2006;279:1–49.
[12] IEA. International energy agency report. Capturing CO_2; 2007.
[13] Goeppert A, Meth S, Prakash GKS, Olah GA. Nanostructured silica as a support for regenerable high-capacity organoamine-based CO_2 sorbents. Energy Environ Sci 2010;3(12):1949–60.
[14] Haszeldine RS. Carbon capture and storage: how green can black be? Science 2009;325:1647–51.
[15] Resnik KP. Aqua ammonia process for simultaneous removal of CO_2, SO_2 and NO_x. Int J Environ Technol Manage 2004;4:89–104.
[16] Choi S, Drese JH, Jones CW. Adsorbent materials for carbon dioxide capture from large anthropogenic point sources. Chem Sustain Chem 2009;2(9):796–854.
[17] Martín CF, García S, Beneroso D, Pis JJ, Rubiera F, Pevida C. Precombustion CO_2 capture by means of phenol-formaldehyde resin-derived carbons: from equilibrium to dynamic conditions. Sep Purif Technol 2012;98:531–8.
[18] Yong Z, Mata V, Rodrigues AE. Adsorption of carbon dioxide at high temperature-a review. Sep Purif Technol 2002;26:195–203.
[19] Chen Z, Deng S, Wei H, Wang B, Huang J, Yu G. Activated carbons and amine-modified materials for carbon dioxide capture — a review. Front Environ Sci Eng 2013;7(3):326–40.
[20] Yu CH, Huang CH, Tan CS. A review of CO_2 capture by absorption and adsorption. Aerosol Air Quality Res 2012;12(5):745–69.
[21] Martín CF, García S, Pis JJ, Rubiera F, Pevida C. Doped phenol-formaldehyde resins as precursors for precombustion CO_2 capture adsorbents. 10th Int Confer Greenhouse Gas Control Technol 2011;4:1222–7.
[22] Martín CF, Plaza MG, Pis JJ, Rubiera F, Pevida C, Centeno TA. On the limits of CO_2 capture capacity of carbons. Sep Purif Technol 2010;74(2):225–9.
[23] Martín CF, Stockel E, Clowes R, Adams DJ, Cooper AI, Pis JJ, Rubiera F, Pevida C. Hypercrosslinked organic polymer networks as potential adsorbents for pre-combustion CO_2 capture. Mater Chem 2011;21(14):5475–83.
[24] Songolzadeh M, Ravanchi MT, Soleimani M. Carbon dioxide capture and storage: a general review on adsorbents. World Acad Sci Eng Technol 2012;70.
[25] Samanta A, Zhao A, Shimizu GKH, Sarkar P, Gupta R. Post-combustion CO_2 capture using solid sorbents: a review. Ind Eng Chem Res 2011;51(4):1438–63.
[26] Xu X, Song C, Andresen JM, Miller BG, Scaroni AW. Novel polyethylenimine-modified mesoporous molecular sieve of MCM-41 type as high-capacity adsorbent for CO_2 capture. Energy Fuels 2002;16(6):1463–9.
[27] Kim S, Ida J, Guliants VV, Lin YS. Tailoring pore properties of MCM-48 silica for selective adsorption of CO_2. J Phys Chem B 2005;109(13):6287–93.
[28] Hicks JC, Drese JH, Fauth DJ, Gray ML, Qi G, Jones CW. Designing adsorbents for CO_2 capture from flue gas-hyperbranched aminosilicas capable of capturing CO_2 reversibly. J Am Chem Soc 2008;130(10):2902–3.
[29] Olea A, Sanz-Pérez ES, Arencibia A, Sanz R, Calleja G. Amino-functionalized pore-expanded SBA-15 for CO_2 adsorption. Adsorption 2013;19(2–4):589–600.
[30] Wei L, Gao Z, Jing Y, Wang Y. Adsorption of CO_2 from simulated flue gas on pentaethylenehexamine-loaded mesoporous silica support adsorbent. Ind Eng Chem Res 2013;52(42):14965–74.
[31] Sanz R, Calleja G, Arencibia A, Sanz-Pérez ES. CO_2 adsorption on branched polyethyleneimine-impregnated mesoporous silica SBA-15. Appl Surf Sci 2010;256(17):5323–8.
[32] Sanz-Pérez ES, Arencibia A, Sanz R, Calleja G. New developments on carbon dioxide capture using amine-impregnated silicas. Adsorption 2016;22:609–19.
[33] Sanz R, Calleja G, Arencibia A, Sanz-Pérez ES. Amino functionalized mesostructured SBA-15 silica for CO_2 capture: exploring the relation between the adsorption capacity and distribution of amino groups by TEM. Microporous Mesoporous Mater 2012;158:309–17.
[34] Knöfel C, Descarpentries J, Benzaouia A, Zeleňák V, Mornet S, Llewellyn PL, Hornebecq V. Functionalised micro-/mesoporous silica for the adsorption of carbon dioxide. Microporous Mesoporous Mater 2007;99(1–2):79–85.
[35] Son WJ, Choi JS, Ahn WS. Adsorptive removal of carbon dioxide using polyethyleneimine-loaded mesoporous silica materials. Microporous Mesoporous Mater 2008;113(1–3):31–40.
[36] Hartono A, Hoff KA, Mejdell T, Svendsen HF. Solubility of carbon dioxide in aqueous 2.5 M of diethylenetriamine (DETA) solution. Energy Procedia 2011;4:179–86.
[37] Kim I. Heat of reaction and VLE of post combustion CO_2 absorbent PhD Thesis. Trondheim, Norway: Norwegian University of Science and Technology; 2009.
[38] Ma L, Bai R, Hu G, Chen R, Hu X, Dai W, et al. Capturing CO_2 with amine-impregnated titanium oxides. Energy Fuels 2013;27(9):5433–9.
[39] Zhao X, Hu X, Hu G, Bai R, Dai W, Fan M, et al. Enhancement of CO_2 adsorption and amine efficiency of Titania modified by moderate loading of diethylenetriamine. J Mater Chem A 2013;1(20):6208–15.

[40] ACSMAterial(R). Advanced Chemicals Supplier <http://www.acsmaterial.com/>; 2014.
[41] Ebner AD, Gray ML, Chisholm NG, Black QT, Mumford DD, Nicholson MA, et al. Suitability of a solid amine sorbent for CO_2 capture by pressure swing adsorption. Ind Eng Chem Res 2011;50(9):5634–41.
[42] Gray ML, Hoffman JS, Hreha DC, Fauth DJ, Hedges SW, Champagne KJ, et al. Parametric study of solid amine sorbents for the capture of carbon dioxide†. Energy Fuels 2009;23(10):4840–4;
Ho YS, Chiang CC. Sorption studies of acid dye by mixed sorbents. Adsorpt J Int Adsorpt Soc 2001;7(2):139–47.
[43] Sing KS, Everett DH, Haul RAW, Moscou L, Pierotti RA, Rouquerol J, et al. Reporting physisorption data for gas/solid systems with special reference to the determination of surface area and porosity (recommendations 1984). Pure Appl Chem 1985;57:603–20.
[44] Serna-Guerrero R, Sayari A. Modeling adsorption of CO_2 on amine-functionalized mesoporous silica. 2: Kinetics and breakthrough curves. Chem Eng J 2010;161(1-2):182–90.
[45] Fan X, Parker DJ, Smith MD. Adsorption kinetics of fluoride on low cost materials. Water Res 2003;37:4929–37.
[46] Weber WJ, Morris JC. Advances in water pollution research: removal of biologically resistant pollutant from wastewater by adsorption. Proceedings of 1st international conference on water pollution symposium, vol. 2. Oxford: Pergamon Press; 1962. p. 231–66.
[47] Weber WJ, Morris JC. Kinetics of adsorption on carbon from solutions. J Sanit Eng Div Am Soc Civ Eng 1963;89:31–60.
[48] Choi JW, Choi NC, Lee SJ, Kim DJ. Novel three-stage kinetic model for aqueous benzene adsorption on activated carbon. J Colloid Interf Sci 2007;314(2):367–72.
[49] Wu FC, Tseng RL, Juang RS. Initial behavior of intraparticle diffusion model used in the description of adsorption kinetics. Chem Eng J 2009;153(1–3):1–8.
[50] Zhao W, Zhang Z, Li Z, Cai N. Investigation of thermal stability and continuous CO_2 capture from flue gases with supported amine sorbent. Ind Eng Chem Res 2013;52(5):2084–93.
[51] Qi G, Wang Y, Estevez L, Duan X, Anako N, Park AHA, et al. High efficiency nanocomposite sorbents for CO_2 capture based on amine-functionalized mesoporous capsules. Energy Environ Sci 2011;4(2):444–52.
[52] Wang J, Long D, Zhou H, Chen Q, Liu X, Ling L. Surfactant promoted solid amine sorbents for CO_2 capture. Energy Environ Sci 2012;5(2):5742–9.
[53] Chaikittisilp W, Kim HJ, Jones CW. Mesoporous alumina-supported amines as potential steam-stable adsorbents for capturing CO_2 from simulated flue gas and ambient air. Energy Fuels 2011;25(11):5528–37.
[54] Chen C, Ahn WS. CO_2 capture using mesoporous alumina prepared by a sol–gel process. Chem Eng J 2011;166(2):646–51.
[55] (a) Xu X, Song C, Andrésen JM, Miller BG, Scaroni AW. Preparation and characterization of novel CO_2 "molecular basket" adsorbents based on polymer-modified mesoporous molecular sieve MCM–41. Microporous Mesoporous Mater 2003;62(1-2):29–45;
(b) Xu X, Song C, Miller BG, Scaroni AW. Adsorption separation of carbon dioxide from flue gas of natural gas-fired boiler by a novel nanoporous "molecular basket" adsorbent. Fuel Process Technol 2005;86(14–15):1457–72.
[56] Prakash DV, Vijaykumar VM. Quickly design CO_2-amine absorber. Indian J Chem Technol 2006;13:47–52.
[57] Zare Aliabad H, Mirzaei S. Removal of CO_2 and H_2S using aqueous alkanolamine solutions. World Acad Sci Eng Technol 2009;3:164–73.
[58] Wang J, Chen H, Zhou H, Liu X, Qiao W, Long D, et al. Carbon dioxide capture using polyethylenimine-loaded mesoporous carbons. J Environ Sci 2013;25(1):124–32.
[59] Yue MB, Chun Y, Cao Y, Dong X, Zhu JH. CO_2 capture by as-prepared SBA-15 with an occluded organic template. Adv Function Mater 2006;16(13):1717–22.
[60] Yue MB, Sun LB, Cao Y, Wang Y, Wang ZJ, Zhu JH. Efficient CO_2 capturer derived from as-synthesized MCM-41 modified with amine. Chem – A Eur J 2008;14(11):3442–51.
[61] Yue MB, Sun LB, Cao Y, Wang ZJ, Wang Y, Yu Q, et al. Promoting the CO_2 adsorption in the amine-containing SBA-15 by hydroxyl group. Microporous Mesoporous Mater 2008;114(1–3):74–81.
[62] Plaza MG, Pevida C, Arenillas A, Rubiera F, Pis JJ. CO_2 capture by adsorption with nitrogen enriched carbons. Fuel 2007;86(14):2204–12.
[63] Plaza MG, Pevida C, Arias B, Fermoso J, Arenillas A, Rubiera F, et al. Application of thermogravimetric analysis to the evaluation of aminated solid sorbents for CO_2 capture. J Therm Anal Calorimetry 2008;92(2):601–6.
[64] Zheng F, Addleman RS, Aardahl CL, Fryxell GE, Brown DR, Zemanian TS. Amine functionalized nanoporous materials for carbon dioxide capture. In: Fryxell Glen E, Cao Guozhong, editors. Chapter 12 in environmental applications of nanomaterials: synthesis, sorbents and sensors. London, United Kingdom: Imperial College Press; 2007. p. 285–312.
[65] Wang D, Sentorun-Shalaby C, Ma X, Song C. High-capacity and low-cost carbon-based "molecular basket" sorbent for CO_2 capture from flue gas. Energy Fuels 2011;25:456–8.
[66] Dubinin MM. Fundamentals of the theory of adsorption in micropores of carbon adsorbents: characteristics of their adsorption properties and microporous structures. Carbon 1989;27(3):457–67.